International Journal of Science and Technology (IJST)
ISSN: 3049-1118, Volume- 2, Issue- 4 (Oct – Dec 2025)

Photocatalytic Activity of Green Synthesis ZnO AND FeO Nanoparticles of Calotropis Gigantea Flower Extract

Benecia Ravi R[1*], J.E. Merlin Sasikala[2]
[1]Bishop Heber College, Tiruchirappalli, Tamilnadu
[2]Associate Professor in Education, Alagappa University College of Education
Alagappa University Karaikudi-3 Sivaganga District, Tamilnadu, India

Abstract

Green Synthesis of Zno and Feo nanoparticles is carried out by Calotropis gigantea flower extract with Zinc Acetate and Ferric Chloride salt. When the aqueous flower extract was put into the FeO Solution it turns into puple to brown colour immediately this indicates the reduction of iron ions in the solution and when the flower extract was put into the ZnO solution it turns into purple to dark green colour immediately this indicates the reduction of zinc ions in the solution. The synthesized FeO and ZnO NPs were characterized by UV, ITIR, XRD, DLS and SEM. It was utilized to determine the crystallinity, shape, and functional group responsible for the capping, reducing, and photocatalytic destruction of synthesized ZnO and FeO NPs. The degradation of Methyl Red and Crystal Violet dye under sunlight, which was used to examine the photocatalysis of synthetic ZnO and FeO NPs.

Keywords: FeO, ZnO, Calotropis gigantea, Photocatalysis

INTRADUCTION

A nanoparticle is a microscopic object having at least one dimension less than 100 nanometres. They have unique optical, thermal, electrical, chemical, and physical characteristics that set them apart from bulk materials. They are therefore used in many different areas, including as consumer goods, heavy industry, chemistry, the environment, energy, agriculture, information technology, and communication. Microorganisms (bacteria, yeast, fungi, algae, and viruses), plants, and other biological resources can be used to create nanoparticles [1]. Due to their narrow band gaps, chemical stability, magnetic properties, and other attributes, iron oxide (FeO) NPs are regarded as excellent materials for environmental and biological applications. A common ferric oxide found in nature is iron oxide, or Fe2O3. Under normal temperature and pressure, It ranks among the most thermodynamically stable iron oxide compounds and has the potential to be mildly magnetic. In nature, iron oxides can take a variety of shapes. The most prevalent types are magnetite (Fe3O4), magnetite (-Fe2O3), and hematite (-Fe2O3). Iron oxide nanomaterials (NMs) with special properties and functions have been intensively investigated in recent years because of their nanoscale size, high surface area to volume ratios, and superparamagnetism. Particularly, the ease with which matter can be synthesised, coated,

*Corresponding Author Email: benciaravir02@gmail.com
Published: 29/11/2025
DOI: https://doi.org/10.70558/IJST.2025.v2.i4.241120

modified, or subjected to atomic-scale control or manipulation could offer unequalled versatility. When paired with biotechnology, iron oxide nanomaterials (NMs) with low toxicity, chemical inertness, and biocompatibility offer great potential. Iron oxide NMs are used because of its special characteristics, which also explain why iron oxide bulk materials differ greatly from one another. Preparation methods and surface coating media are believed to have a major impact on the size distribution, shape, magnetic characteristics, surface chemistry, and ease of synthesis, coating, or modification, as well as the possibility for manipulation. Although NMs are thought to have a tendency to congregate in solution, colloidal nanoparticle stability is frequently affected by van der Waals and electrostatic interactions. Changing iron oxide nanomaterials (NMs) is an interesting potential tactic since NMs can react with different functional groups. The stability of iron oxide colloid suspensions can be greatly enhanced by surface-modifying them with the proper functional groups, such as amine, phosphoric acid, and carboxylic acid. Functionalizing with various media would be essential since the type of altered medium determines the actual applicability. A range of media can be used to add various functional groups to iron oxide nanoparticles; Nevertheless, a trustworthy method has not yet been developed and validated. Even in industrial settings, sterically stabilized nanoparticles usually maintain a good dispersion. It should be noted that the intrinsic characteristics of iron oxide nanomaterials (NMs), which are mostly dependent on the manufacturing method and modification media, are closely related to their use. Iron oxide nanoparticles (NMs) have the potential to treat wastewater on an industrial scale due to their low cost, high adsorption capacity, ease of separation, and improved stability. Both laboratory and field testing have shown that iron oxide NMs are efficient at eliminating contaminants. Iron oxide NMs, a kind of nanosorbent or immobilization carrier, are currently employed in two distinct technologies for the remediation of contaminated water: (a) photocatalytic technologies and (b) adsorptive/immobilization technologies. In the former, pollutants are broken down or changed into a less hazardous form using iron oxide nanoparticles as photocatalysts. However, it should be noted that many technologies could employ both approaches. An excellent illustration of excellence is the iron oxide NMs. Fe3O4 nanoparticles were found to have a maximum adsorption capacity for Pb(II) ions of 36.0 mg g1, which was considerably greater than that of previously reported inexpensive adsorbents. The small size of the Fe3O4 nanosorbents facilitated the diffusion of metal ions from solution onto the surface's active areas. For the rapid removal and recovery of metal ions from wastewater effluents, Fe3O4 nanosorbents were proposed as effective and reasonably priced adsorbents. One of the cutting-edge physico-chemical technologies used in the photodegradation of organic contaminants is photocatalysis, which has garnered a lot of interest lately. Iron oxide NM is an excellent photocatalyst for absorbing visible light. In contrast to the widely used TiO2, which mainly absorbs UV light with wavelengths of b380 nm (covering only 5% of the solar spectrum) due to its wide band-gap of 3.2 eV, Fe2O3 is an intriguing n-type semiconducting material with a band-gap of 2.2 eV and a good candidate for photodegradation under visible light conditions. The substantial generation of electron-hole pairs brought on by the narrow band-gap light may be the reason for iron oxide NMs' better photocatalytic performance than TiO2. Many Fe(III) oxide species, such as -Fe2O3, -Fe2O3, -FeOOH, -FeOOH, and -FeOOH, have been suggested to break down organic pollutants and reduce their toxicity due to their improved photocatalytic action. These NMs are illustrations of a new technique for modifying

the catalytic properties of iron oxide for photocatalysis, resulting in a safe and effective nanotechnology for wastewater treatment. The photodegradation of the dye Congo red (CR) (C32H24N6O6S2) by iron oxide nanoparticles made by co-precipitation and thermal evaporation is one example. The maximum removal efficiency was 96% at a size of 100 nm. Furthermore, it was found that while the rate of degradation was enhanced in the presence of light, irradiation had little to no effect on the catalytic decomposition capability [2].

ZnO NP is one of the semiconducting materials whose structure is part of the P63 space group. ZnO NP also has effective light-trapping properties and high visible-range transparency. Good photocatalysis, natural abundance, and non-toxicity are just a few of its many advantages. The ZnO NP plays a major role in the mechanisms behind toxicity by inhibiting immune cells. ZnO NPs have stronger catalytic organic conversions than other nanoparticles because of their environmental tolerance and rapid and simple production. By changing the photodynamic effect of sensors, ZnO NPs have a major impact on electrochemistry. Zinc oxide nanoparticles often include neutral hydroxyl groups on their surface, which is crucial for their surface charge behavior. In an aqueous medium with a high pH, the chemisorbed protons (H+) depart from the particle surface, leaving a negatively charged surface with partially bonded oxygen atoms (ZnO-) [3]. At lower pH levels, protons from the surrounding environment are probably carried to the particle surface, where they cause surface ZnOH2+ groups to become positively charged. The isoelectric point of 9–10 indicates that ZnO nanoparticles will have a significant positive surface charge under physiological conditions. The primary features of ZnO NPs are their non-toxicity, hygroscopicity, affordability, and ease of access, given that cancer cells typically have large membrane potentials and an abundance of anionic phospholipids on their outer membrane. It is one of the safest materials to use as a catalyst in various organic processes. Scientists regarded ZnO NPs as some of the best metal nanoparticles in the world because of their extensively researched optical and electrochemical characteristics. ZnO NPs have been employed in sensors because of their semiconducting properties and linear band gap (3.37 eV). It was found that ZnO NPs are a useful material for identifying a few of the dangerous gasses that are present in the environment. The scientific community is interested in these ZnO NPs because they are stable under UV radiation, while being one of the less expensive n-type semiconductors. Furthermore, the ZnO NPs degrade toxic colors like rhodamine B and malachite green. These dangerous substances can be eliminated from the environment in a few different methods, but they are all expensive and time-consuming. As a result, green nanoparticle synthesis and its usage in degradation have emerged in research on nanoparticles and their applications, including their use as probiotic spore tablets. The ZnO NPs can display extra characteristics and be bonded to different transition metal oxide nanoparticles when there is an anisotropic distribution of functional surface charges. ZnO NPs have a higher antibacterial effect as the concentration increases. E. coli, S. aureus, P. aeruginosa, Candida albicans, and A. brasiliensis were the five disease-causing pathogens whose antimicrobial activity was evaluated using the disc diffusion and broth dilution procedures. These pathogens' MIC and MBC were subsequently ascertained. ZnO NPs were found to exhibit concentration-dependent good activity for all five illnesses. It implies a close relationship between ZnO NP concentrations and the mechanism of antibacterial action. The ZnO NPs were produced by photocatalytically

breaking down malachite green, a dye that is also thought to be carcinogenic, using R. pyridinivorans NT2 actenobacteria. The malachite green dye did not considerably deteriorate during the control procedure, although the dye exhibits an absorbance peak at 623 nm. The maximum photocatalytic activity was seen at two hours, and it remained constant without showing any further degrading processes. Furthermore, the chemically stable ZnO NPs were used as catalysts for condensation reactions. The researchers employed Poncirus trifoliata to produce the ZnO NPs, which were then confirmed by a number of analytical techniques. Agglomeration particles with sizes ranging from 8.48 to 32.51 nm were found in the results. The photocatalytic degradation capacity of the biogenic ZnO NP under direct sunlight was tested using methylene blue (10 mg/L) in an aqueous solution.

MATERIALS AND METHODS

Chemicals and Reagents

Zinc Acetate, Ferric Chloride, Calotropis gigantea flower Extract.

Collection and Extraction of plant material

Green Synthesis of Iron Oxide Nanomaterial

Material Required

Test sample (CG), Double distilled water, Iron (III) chloride and Centrifuge tube.

Procedure

Plant extract (CG) and iron (III) chloride were used to synthesize iron nanoparticles. Iron (III) chloride in double-distilled water at 0.1 M. The ratios of iron (III) chloride to plant extract (CG) were 5:5, 6:4, 7:3, 8:2, and 9:1.

Iron Oxide Nanomaterial synthesis

Figure.1 *Plant extract (CG)*

Figure 2 *0.1 M of Iron (III) chloride*

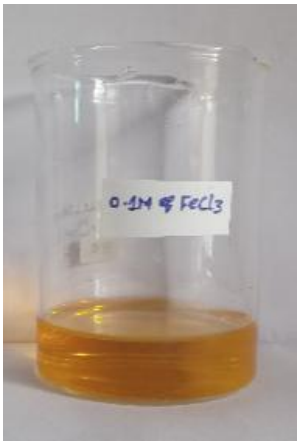

Figure.3 *Synthesis of FeO NPs using Iron (III) chloride + (CG) Plant extract in a different ratio*

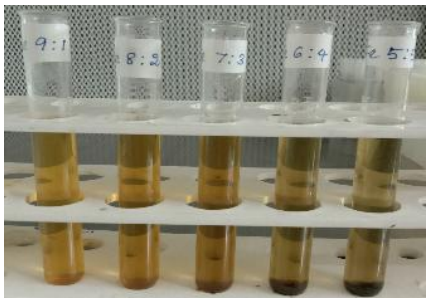

Figure.4 *Bulk production using Iron (III) chloride + (CG) plant extract*

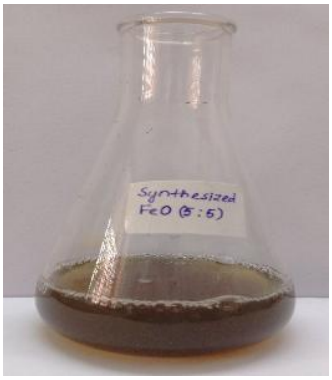

Figure 5. *Synthesized FeO NPs*

Green Synthesis of Zinc Oxide Nanomaterial

Material Required

Test sample (CG), Double distilled water, Zinc acetate and Centrifuge tube.

Procedure

Zinc acetate and plant extract were used in the synthesis of zinc nanoparticles (CG). Double-distilled water with 0.1 M zinc acetate.

Zinc Oxide Nanomaterial synthesis

Figure 6 *Plant extract (CG)*

Figure.7 *0.1 M of Zinc acetate*

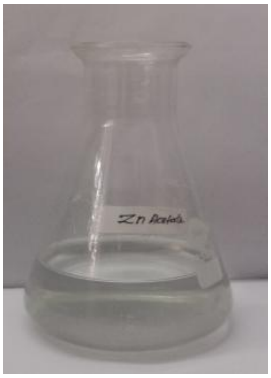

Figure 8 *Bulk production using Zinc acetate + (CG) plant extract*

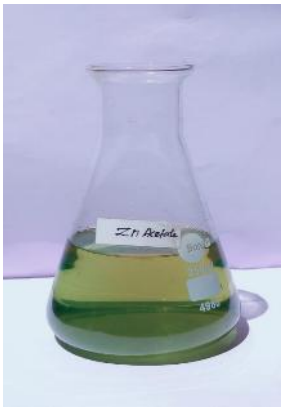

Figure 9 *Synthesized ZnO NPs*

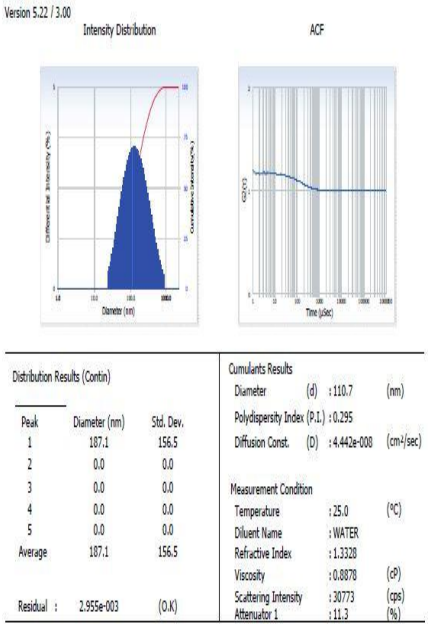

Characterization

DLS of FeO Nanoparticle

DLS Of ZnO Nanoparticle

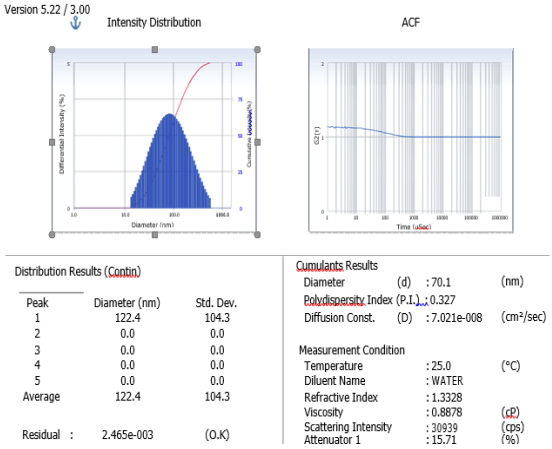

FTIR of FeO Nanoparticle

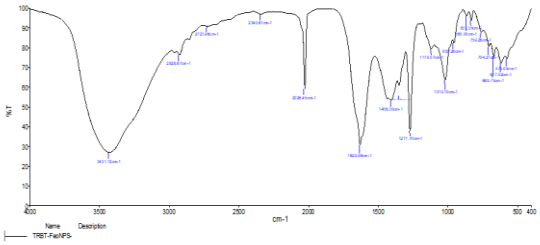

FTIR Of ZnO Nanoparticle

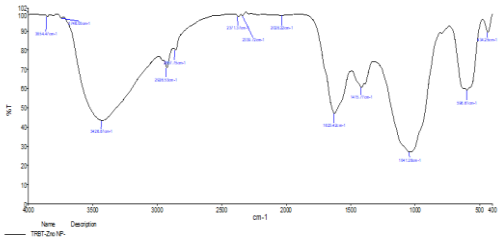

XRD Of FeO Nanoparticle

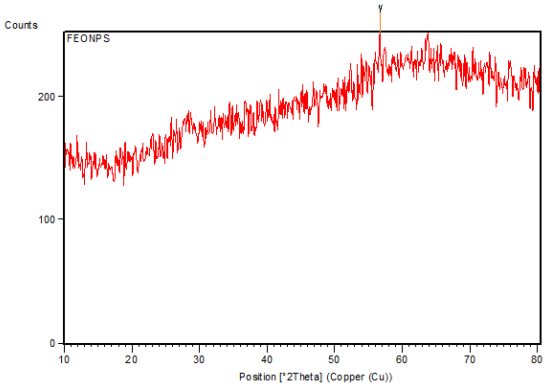

XRD of ZnO Nanoparticle

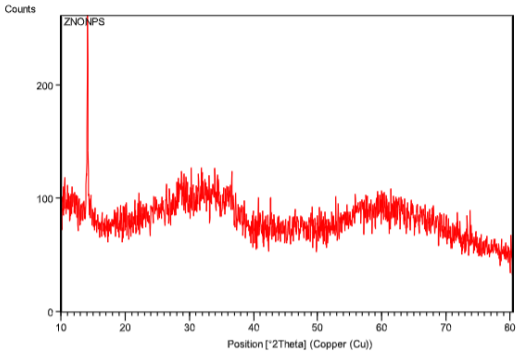

SEM of FeO Nanoparticle

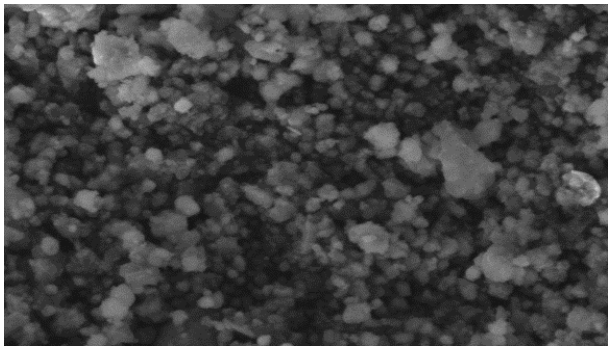

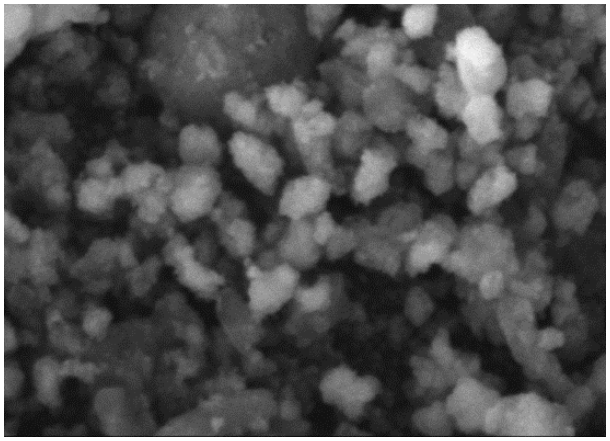

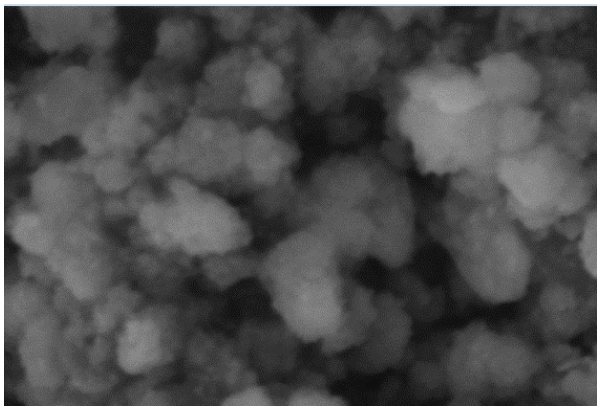

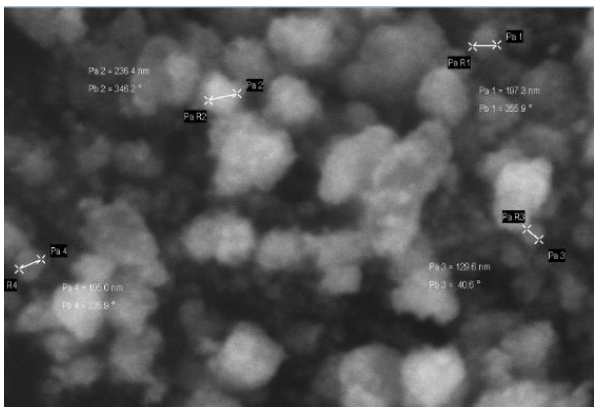
Pa 1
Pa R1
Pa 2
Pa R2
Pa R3
Pa 3
Pa 4
R4

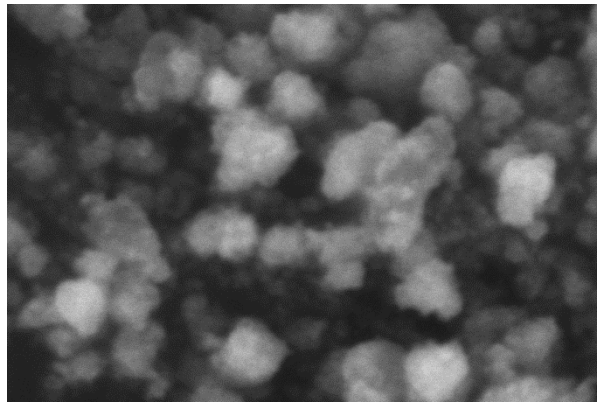

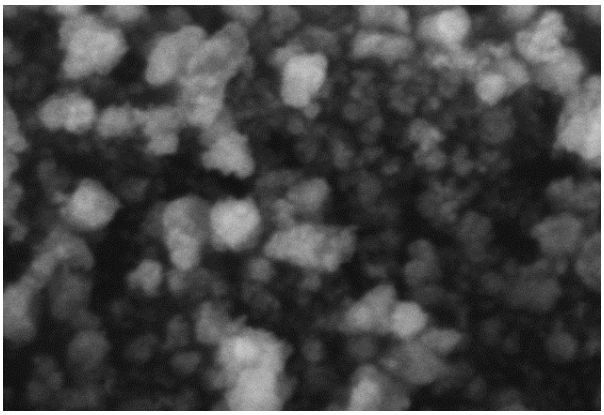

SEM of ZnO Nanoparticle

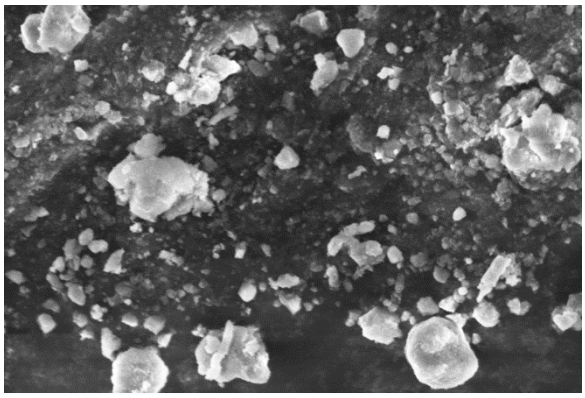

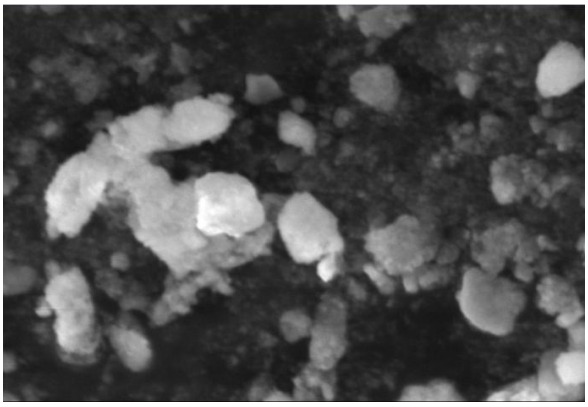

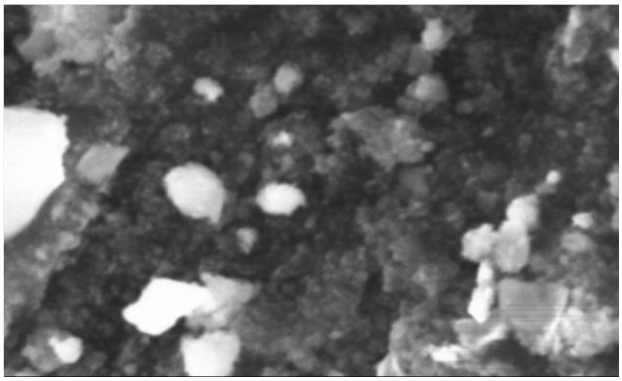

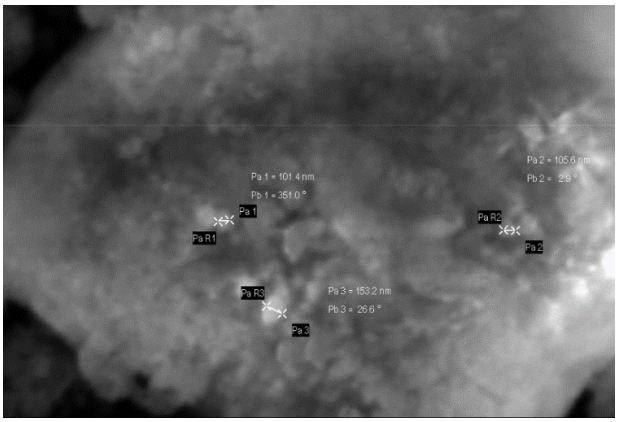
Pa 1 = 101.4 nm
Pb 1 = 351.0 °
Pa 1
Pa R1
Pa 2 = 105.6 nm
Pb 2 = 2.9 °
Pa R2
Pa 2
Pa R3
Pa 3 = 153.2 nm
Pb 3 = 26.6 °
Pa 3

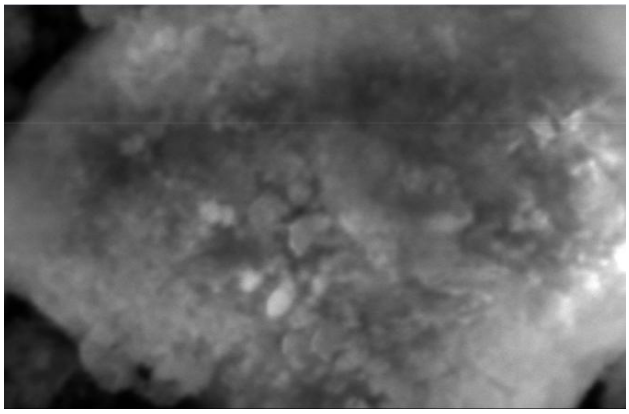

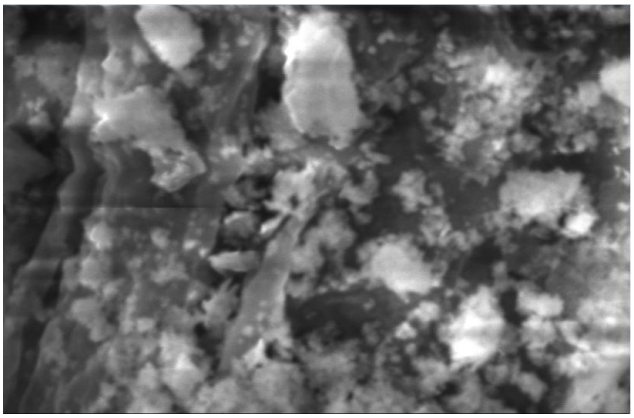

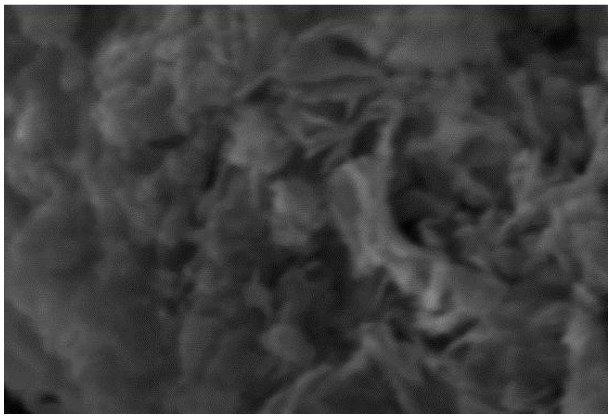

UV – VISIBLE SPECTROSCOPY ANALYSIS OF FeO NANOPARTICLE

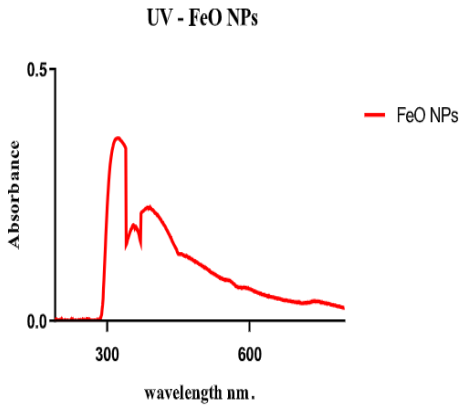

Photocatalytic Activity

FeO Nanoparticle

Methyl Red dye

Procedure

The elimination of Methyl red dyes (10 ml of aqueous solution of dyes dissolved 0.05g) under UV or sunlight radiation was used to assess the photo-catalytic behavior of the produced FeONPs (sample). A 150 W Xe (Xenon) lamp served as the light source, and the photo-reaction vessel was 10 cm away from the UV source. The suspensions were magnetically agitated for 30 minutes in the dark before being exposed to radiation. After that, the photoreaction vessel was subjected to UV radiation in a typical ambient setting. In the photo-removal experiment, the chosen dyes were combined with 50 mg of catalyst sample EeONPs. Three milliliters of the suspension were obtained at regular intervals for centrifugation to extract the photorcatalyst and for additional analysis using a UV-Vis absorption spectrometer. The following equation was used to get the photo-removal efficiency percentage. The permanence of the photocatalytic sample was then examined by five repeated cycles of recycling tests (0, 1, 2, 3, 4, and 5 hours). Before being used again for the subsequent

experiment, the composite catalyst was centrifuged, cleaned with ethanol and deionized water, and dried. The following equation was used to get the photo-removal efficiency percentage:

% Photo-removal efficiency = C_0 - $C/C_0 \times 100$

where C0 represents the starting dye concentration and C represents the final dye concentration following photo-irradiation.

S. No	OD Value at different Time interval (hours)	Test sample concentration (µg/ml)					
		Control	500 µg/ml	250 µg/ml	100 µg/ml	50 µg/ml	10 µg/ml
1.	Initial	1.188	0.889	0.953	0.948	1.032	1.085
2.	1 hr	1.172	0.889	0.931	0.889	0.981	1.053
3.	2 hrs	0.296	0.121	0.123	0.126	0.130	0.139
4.	3 hrs	0.267	0.110	0.118	0.121	0.137	0.155
5.	4 hrs	0.260	0.109	0.114	0.115	0.128	0.140
6.	5 hrs	0.259	0.105	0.113	0.118	0.120	0.127

% of different Time interval (hours)	% of Test sample concentration (µg/ml)					
	Control	500µg/ml	250µg/ml	100µg/ml	50µg/ml	10 µg/ml
Initial	100	25.16835	19.78114	20.20202	13.13131	8.670034
1 hr	1.346801	25.16835	21.633	25.16835	17.42424	11.36364
2 hrs	75.08418	89.81481	89.64646	89.39394	89.05724	88.29966

3 hrs	77.52525	90.74074	90.06734	89.81481	88.46801	86.95286
4 hrs	78.11448	90.82492	90.40404	90.31987	89.22559	88.21549
5 hrs	78.19865	91.16162	90.48822	90.06734	89.89899	89.30976

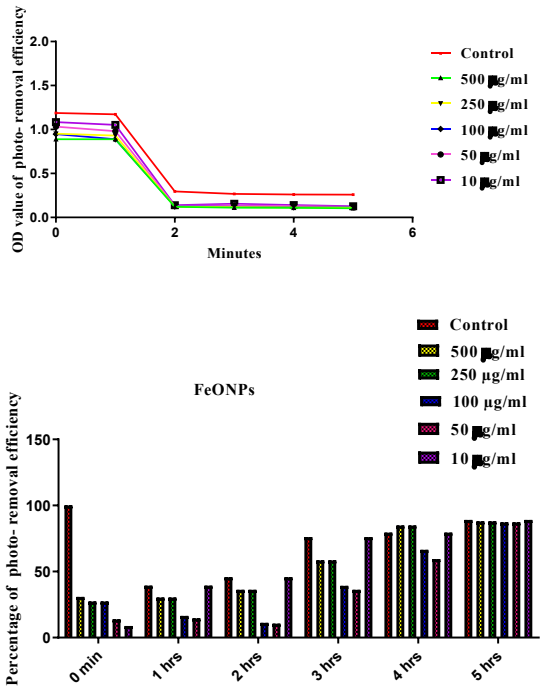

Crystal violet Dye

Procedure

The elimination of crystal violet dyes (10 ml of water solution of dyes dissolved 0.05g) under UV or solar radiation was used to assess the photo-catalytic behavior of the produced FeONPs (sample). The photo-reaction vessel was 10 cm away from the UV source, which was a 150 W Xe (Xenon) lamp. The suspensions underwent 30 minutes of magnetic stirring in the dark prior to radiation. After that, at typical ambient circumstances, the photoreaction vessel was exposed to UV radiation. In the photo-removal experiment, 50 mg of catalyst sample EeONPs was combined with the chosen colors. Three milliliters of the suspension were obtained at regular intervals for centrifugation to extract the photorcatalyst and for additional analysis using a UV-Vis absorption spectrometer. The following equation was used to get the photo-removal efficiency percentage. The permanence of the photocatalytic sample was then examined by five repeated cycles of recycling tests (0, 1, 2, 3, 4, and 5 hours). Before being used again for the subsequent experiment, the composite catalyst was centrifuged, cleaned with ethanol and deionized water, and dried. The following equation was used to get the photo-removal efficiency percentage:

% Photo-removal efficiency = C_0 - C/C_0× 100

where C0 is the dye's initial concentration and C is its ultimate concentration following photo-irradiation.

S. No	OD Value at different Time interval (hours)	Test sample concentration (µg/ml)					
		Control	500 µg/ml	250 µg/ml	100 µg/ml	50 µg/ml	10 µg/ml
1.	Initial	1.049	0.726	0.762	0.762	0.904	0.957
2.	1 hr	1.019	0.636	0.731	0.731	0.876	0.896
3.	2 hrs	0.989	0.510	0.610	0.610	0.871	0.878
4.	3 hrs	0.707	0.251	0.436	0.436	0.638	0.669
5.	4 hrs	0.507	0.216	0.159	0.159	0.352	0.426
6.	5 hrs	0.150	0.115	0.126	0.126	0.134	0.135

S. No	% of different Time interval (hours)	% of Test sample concentration (µg/ml)					
		Control	500µg/ml	250µg/ml	100µg/ml	50µg/ml	10 µg/ml
1.	Initial	100	30.79123	27.35939	27.35939	13.82269	8.770257
2.	1 hr	2.859867	30.31459	30.31459	16.4919	14.58532	39.37083
3.	2 hrs	5.719733	36.12965	36.12965	11.24881	10.58151	45.66254

4.	3 hrs	32.60248	58.43661	58.43661	39.18017	36.22498	76.07245
5.	4 hrs	51.66826	84.84271	84.84271	66.44423	59.3899	79.40896
6.	5 hrs	85.70067	87.98856	87.98856	87.22593	87.1306	89.03718

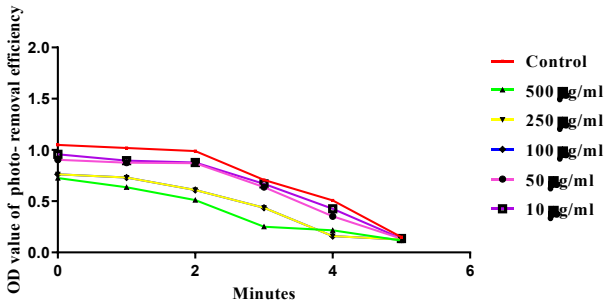

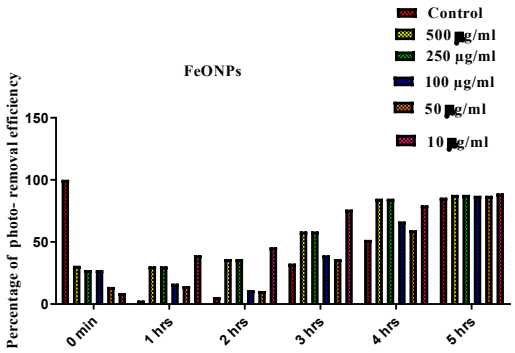

Antifungal Activity of FeO and ZnO Nanoparticles

AGAR WELL DIFFUSION TECHNIQUE

PRINCIPLE

In a plate that had just been seeded with the test organisms, the anti-fungal agent contained in the sample was allowed to diffuse out into the medium and interact. Because there will be a confluent lawn of growth, the resulting zones of inhibition will be evenly round. Millimeters can be used to measure the zone of inhibition's diameter.

MATERIALS REQUIRED

Amphotericin B antimycotic solution, potato dextrose agar medium, beakers, conical flasks, test tubes, spirit lamps, double-distilled water, and petri dishes.

1. AGAR-WELL DIFFUSION TECHNIQUE

a. Agar Medium with Potato Dextrose

In 100 milliliters of distilled water, 20 grams of potato influsion, 2 grams of dextrose, and 1.5 grams of agar were dissolved to create the potato dextrose agar medium. The dissolved medium was autoclaved for 15 minutes at 121°C and 15 pounds of pressure. While still molten, the autoclaved mixture was thoroughly mixed and transferred to 100 mm petri dishes (25–30 ml each plate).

PROCEDURE

Aspergillus niger, Aspergillus flavus, Aspergillus fumigatus, and Cryptococcus neoformans were cultured for 72 hours in Petri plates containing 20 milliliters of potato dextrose agar medium. The wells were then cut, and various concentrations of sample ZnoNPs and FeONPs (500, 250, 100, and 50 µg/ml) were added. Next, the plates were incubated for 72 hours at 28°C. The diameter of the inhibition zone that developed around the wells was used to gauge the anti-fungal action. The positive control was amphotericin B. Graph Pad Prism 6.0 software was used to calculate the values (USA).

Results

Fig : 1 Sample ZnONPs' impact on Aspergillus niger.

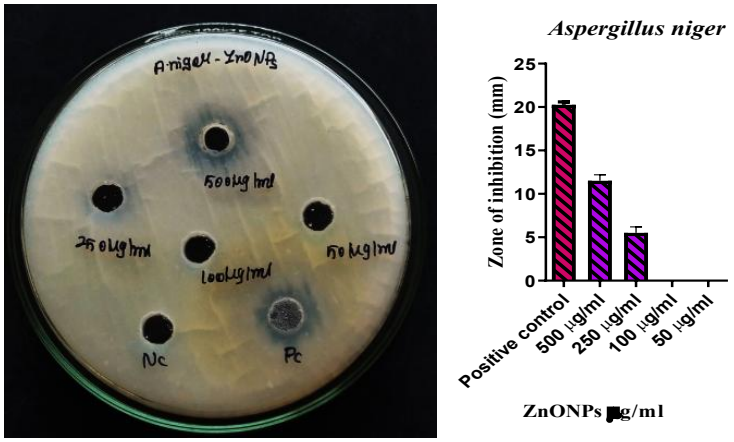

Fig : 2 Sample FeONPs' impact on Aspergillus flavus

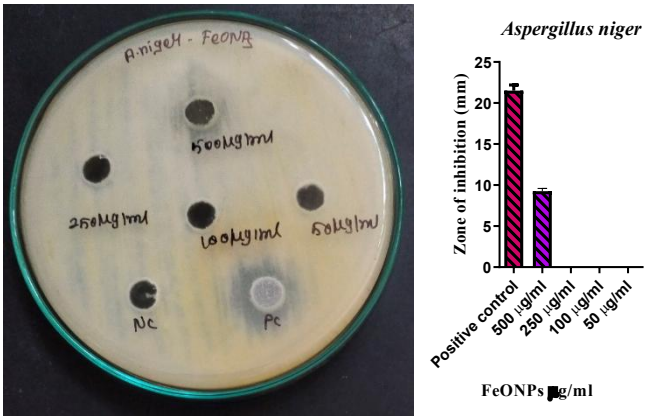

Fig : 3 Sample ZnONPs' impact on Aspergillus flavus.

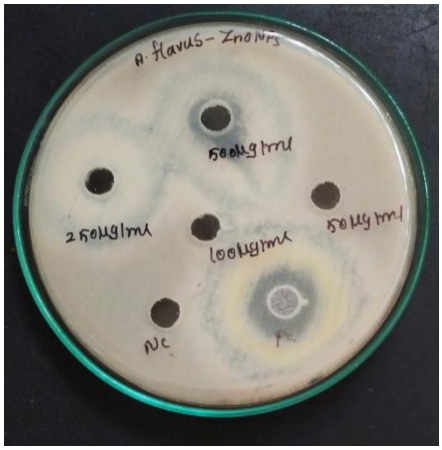

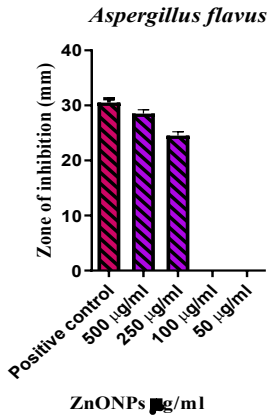

Fig : 4 Sample FeONPs' impact on Aspergillus flavus.

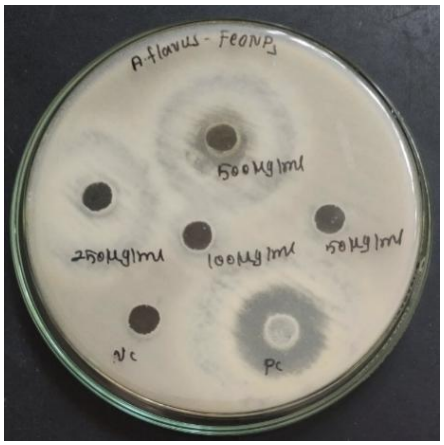

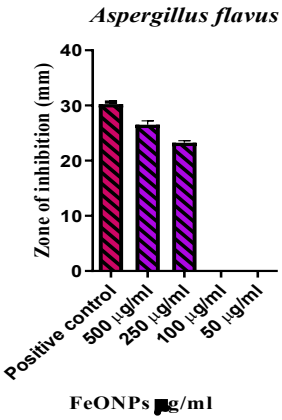

Fig : 5 Sample ZnONPs' impact on Aspergillus fumigatus.

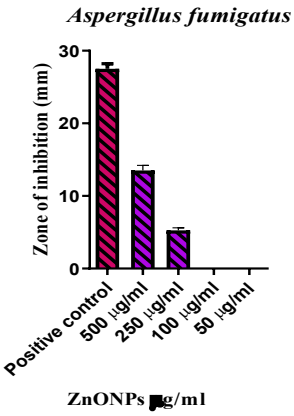

Fig : 6 Sample FeONPs' impact on Aspergillus fumigatus.

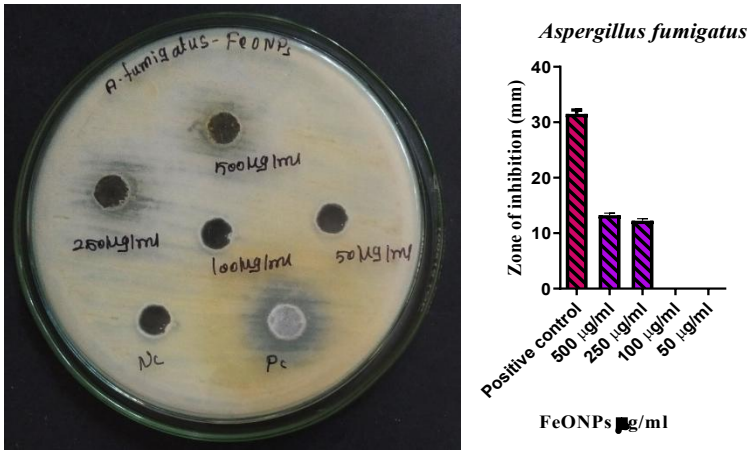

Fig : 7 Sample ZnONPs' impact on Cryptococcus neoformans.

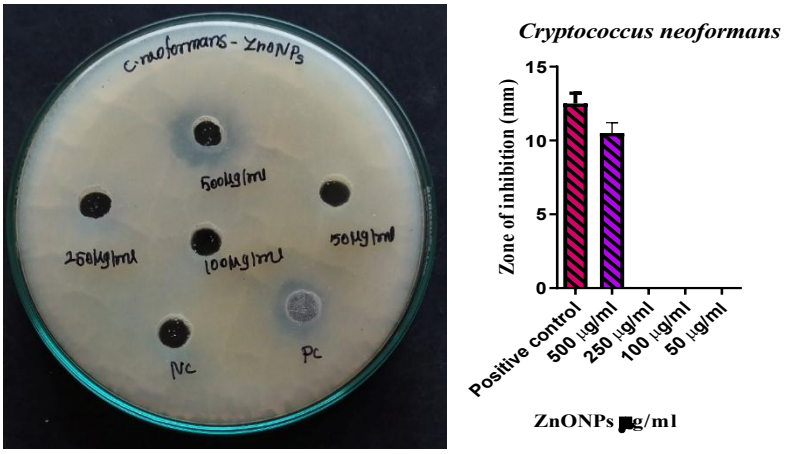

Fig : 8 Sample FeONPs' effects on Cryptococcus neoformans.

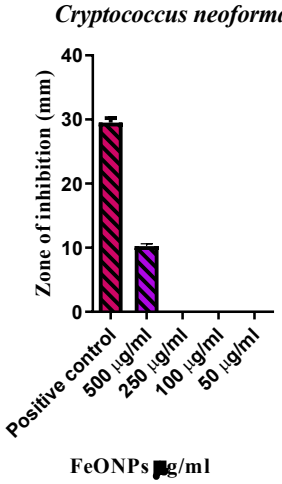

Table 1. SD± Means of the zone of inhibition that sample FeONPs and ZnONPs produced against Cryptococcus neoformans, Aspergillus niger, Aspergillus flavus, and Aspergillus fumigatus.

			Zone of inhibition (mm)

S.NO	The test organism's name	The test sample's name	SD ± Mean				
			500 µg/ml	250 µg/ml	100 µg/ml	50 µg/ml	PC
1	*Aspergillus niger*	ZnONPs	11.5±0.707	5.5±0.70	0	0	20.25 ±0.35
2		FeONPs	9.25±0.35	0	0	0	21.5± 0.70
3	*Aspergillus flavus*	ZnONPs	28.5±0.707	24.5±0.707	0	0	30.5± 0.7
4		FeONPs	26.5±0.70	23.25± 0.3	0	0	30.25 ±0.35
5	*Aspergillus fumigatus*	ZnONPs	13.5±0.7071	5.25±0.35	0	0	27.5± 0.70
6		FeONPs	13.25±0.35	12.25± 0.3	0	0	31.5± 0.707
7	*Cryptococcus neoformans*	ZnONPs	10.5±0.7071	0	0	0	12.5± 0.7071
8		FeONPs	10.25±0.35	0	0	0	29.5± 0.707

SD , *Significance - $p< 0.05$

References

De Magaldi, Silvia W., and Teresa Camero. "Suceptibilidad de Candida albicans" In vitro" mediante los posos de difusión." *Bol. venez. infectol* (1997): 5-8.

Clinical and Laboratory Standards Institute. "Reference method for broth dilution antifungal susceptibility testing of yeasts." *Approved standard M27-A3* (2008).

Antibacterial Activity of FeO and ZnO Nanoparticles

AGAR WELL DIFFUSION METHOD

PRINCIPLE

In a plate that had just been seeded with the test organisms, the antimicrobials in the provided sample were allowed to permeate out into the medium and interact. There will be a confluent lawn of growth, which will result in consistently circular zones of inhibition. Millimeters can be used to quantify the zone of inhibition's diameter.

MATERIALS REQUIRED

(*E. coli, 443, Pseudomonas aeruginosa, 424, Streptococcus oralis, 2696, and Staphylococcus aureus, 902*) were acquired from MTCC, Chandihar, India. Gentamicin antibiotic solution, nutrient broth, and nutrient agar medium were acquired from Himedia, India. Beakers, conical flasks, test tubes, petri dishes, and test samples came from Borosil in India. Spirit lamp and double-distilled water.

1. AGAR- WELL DIFFUSION METHOD

b. Nutrient Agar Medium

In 100 milliliters of distilled water, 2.8 grams of the commercially available Nutrient Agar Medium (HiMedia) were dissolved to create the medium. For fifteen minutes, the dissolved medium was autoclaved at 121°C with fifteen pounds of pressure. After thoroughly mixing the autoclaved media, 25–30 milliliters per 100 mm petriplate were filled while it was still hot.

c. Nutrient broth

To make nutritional broth, 2.8 g of commercially available nutrient medium (HiMedia) was dissolved in 100 ml of distilled water and heated until the medium was completely dissolved. The medium was distributed as needed and autoclaved for 15 minutes at 15 pounds of pressure (121 degrees Celsius) to sterilize it.

1.1.PROCEDURE

A 24-hour culture of bacterial strains (Staphylococcus aureus, 902, E. coli, 443, Pseudomonas aeruginosa, 424, and Streptococcus oralis, 2696) was seeded into Petri plates with 20 milliliters of nutritional agar medium and adjusted to a 0.5 OD value in accordance with the McFarland standard. Concentrations of sample FeONPs and ZnONPs (500, 250, 100, and 50 µg/ml) were introduced after wells were cut. After that, the plates were incubated for twenty-four hours at 37°C. By measuring the diameter of the inhibitory zone that developed around the wells, the antibacterial activity was evaluated. As a positive control, the antibiotic

gentamicin was employed. Graph Pad Prism 6.0 software (USA) was used to compute the data.

Results

Fig : 1 Impact of sample FeONPs against *Staphylococcus aureus.*

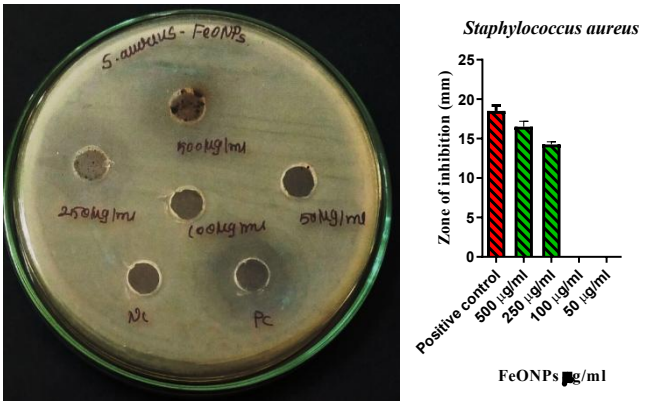

Fig : 2 Impact of sample FeONPs against *E.coli.*

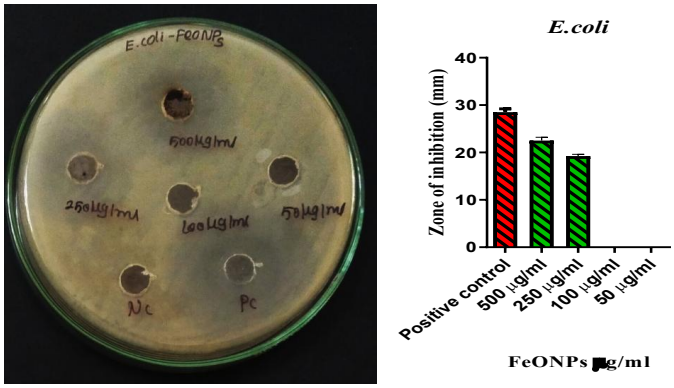

Fig : 3 Impact of sample FeONPs against *Streptococcus oralis.*

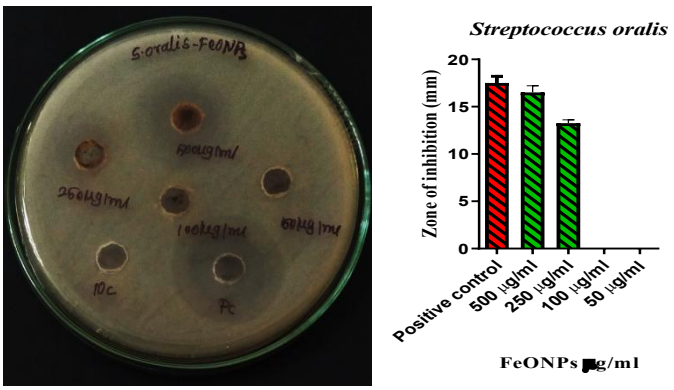

Fig : 4 Impact of sample FeONPs against *Pseudomonas aeruginosa.*

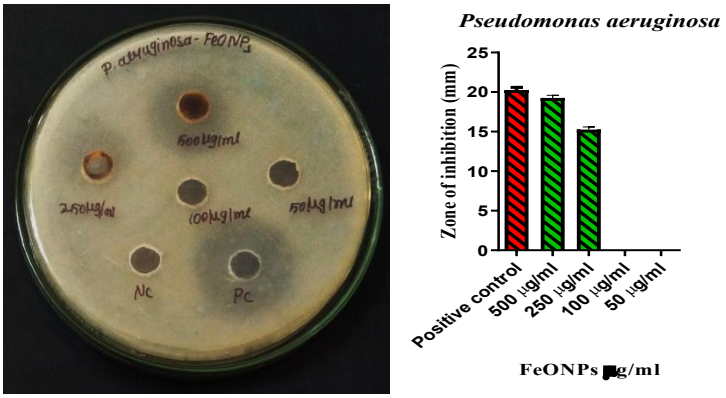

Fig : 5 Sample ZnONPs' impact on Staphylococcus aureus.

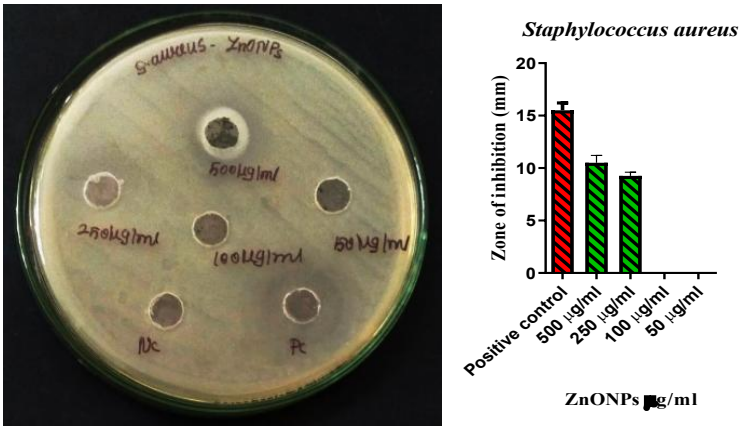

Fig : 6 Impact of sample ZnONPs against E.coli.

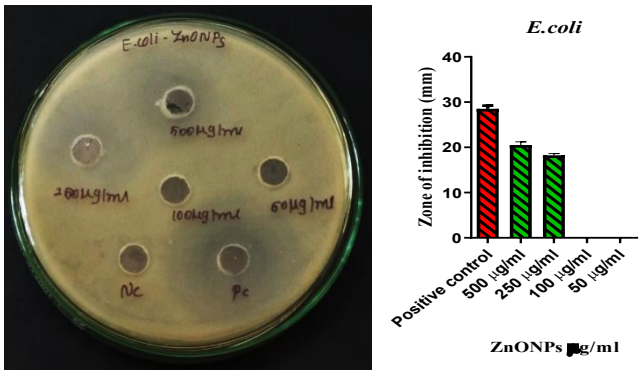

Fig : 7 Sample ZnONPs' impact on Streptococcus oralis.

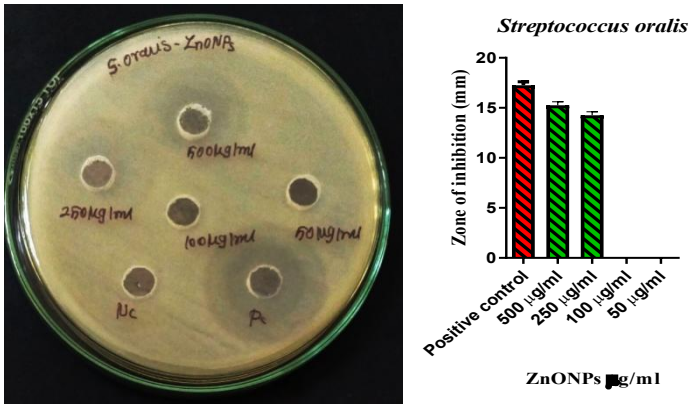

Fig : 8 Pseudomonas aeruginosa is affected by sample ZnONPs.

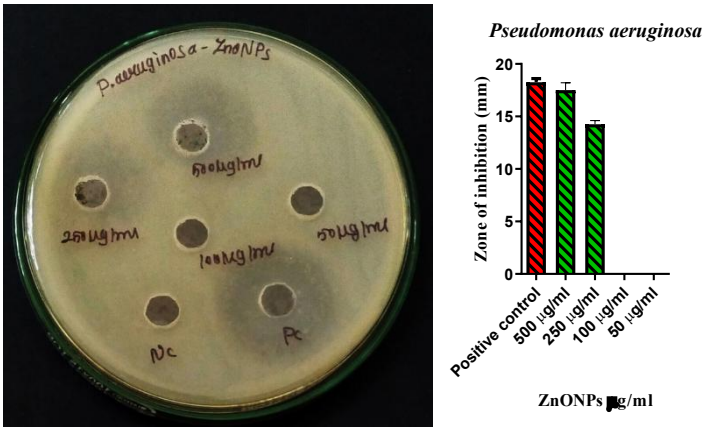

Table 1. SD± Means of the zone of inhibition that the sample FeONPS and ZnONPs produced against Pseudomonas aeruginosa, Streptococcus oralis, E. coli, and Staphylococcus aureus.

S. No	Test organism's name	The test sample's name	Zone of inhibition (mm) SD ± Mean				
			500 µg/ml	250 µg/ml	100 µg/ml	50 µg/ml	PC
1.	*Staphylococcus aureus*	FeONPs	16.5±0.707	14.25±0.35	0	0	18.5±0.707
2.	*E.coli*		22.5±0.70	19.25±0.35	0	0	28.5±0.70
3.	*Streptococcus oralis*		16.5±0.7071	13.25±0.3	0	0	17.5±0.7071
4.	*Pseudomonas aeruginosa*		19.25±0.35	15.25±0.3	0	0	20.25±0.35
5.	*Staphylococcus aureus*	ZnONPs	10.5±0.7071	9.25±0.35	0	0	15.5±0.7
6.	*E.coli*		20.5±0.70	18.25±0.350	0	0	28.5±0.70
7.	*Streptococcus oralis*		15.25±0.35	14.25±0.35	0	0	17.25±0.3

8.	*Pseudomonas aeruginosa*		17.25± 0.35	14.25±0.3	0	0	18.25 ±0.30

SD, *Significance - $p< 0.05$

Conclusion

The paper effectively illustrates the green synthesis of ZnO and FeO nanoparticles employing floral extract from Calotropis gigantea as a natural capping and reducing agent. The immediate color changes during synthesis confirmed the reduction of metal ions, and characterization techniques (UV, FTIR, XRD, DLS, SEM) revealed the nanoparticles' crystallinity, morphology, and functional groups. The synthesized ZnO and FeO nanoparticles exhibited effective photocatalytic activity, efficiently degrading Methyl Red and Crystal Violet dyes under sunlight. This eco-friendly and cost-effective approach offers a sustainable alternative to chemical synthesis, producing biocompatible nanoparticles with potential applications in wastewater treatment, environmental remediation, and other multifunctional uses.

Compliance with Ethical Standards

Conflict of interest

The authors declare that they have no conflict of interest.

Human and Animal Rights

This article does not contain any studies with human or animal subjects performed by any of the authors.

Informed Consent

Informed consent does not apply as this was a retrospective review with no identifying patient information.

Funding: Not applicable

Conflicts of interest Statement: Not applicable

Consent to participate: Not applicable

Consent for publication: Not applicable

Availability of data and material:

Data sharing is not applicable to this article as no new data were created or analyzed in this study.

Code availability: Not applicable

Competing Interests: Not applicable

REFERENCES:

1. Mihir Herlekar,1 Siddhivinayak Barve,1 and Rakesh Kumar2 Plant-Mediated Green Synthesis of Iron Nanoparticles Hindawi Publishing Corporation Journal of Nanoparticles Volume 2014, Article ID 140614, 9 pages
2. Piao Xu a,b , Guang Ming Zeng a,b, ∗, Dan Lian Huang a,b, ∗, Chong Ling Feng a,b , Shuang Hu c , Mei Hua Zhao a,b , Cui Lai a,b , Zhen Wei a,b , Chao Huang a,b , Geng Xin Xie a,b , Zhi Feng Liu a,b Use of iron oxide nanomaterials in wastewater treatment
3. Gunabalan Madhumitha1 & Ganesh Elango1 & Selvaraj Mohana Roopan1 Biotechnological aspects of ZnO nanoparticles: overview on synthesis and its applications
4. Nagarajan S, Kuppusamy KA (2013) Extracellular synthesis of zinc oxide nanoparticle using seaweeds of gulf of Mannar, India. J Nanobiot 11:11–39
5. Pasquet J, Chevalier Y, Couval E, Bouvier D, Noizet G, Morliere C, Bolzinger MA (2014) Antimicrobial activity of zinc oxide particles on five micro-organisms of the challenge tests related to their physicochemical properties. Int J Pharma 460:92–100
6. John W Rasmussen, et al, Zinc oxide nanoparticles for selective destruction of tumor cells and potential for drug delivery applications
7. Mahboob Alam* Photocatalytic activity of biogenic zinc oxide nanoparticles: In vitro antimicrobial, biocompatibility, and molecular docking studies
8. Qu F, Morais PC. Energy levels in metal oxide semiconductor quantum dots in water-based colloids. J Chem Physics 1999;111:8588-94
9. Qu F, Morais PC. The pH dependence of the surface charge density in oxide-based semiconductor nanoparticles immersed in aqueous solution. IEEE Trans Magn 2001;37:2654-6
10. Degen A, Kosec M. Effect of pH and impurities on the surface charge of zinc oxide in aqueous solution. J Europena Ceramic Soc 2000;20:667-73
11. Sun C, Fang C, Stepherr Z, et al. Tumor-targeted drug delivery and MRI contrast enhancement by chlorotoxin-conjugated iron oxide nanoparticles. Future Med 2008;3:495-505
12. Patil S, Reshetnikov S, Haldar MK, et al. Surface-derivatized nanoceria with human carbonic anhydrase II inhibitors and fluorophores: a potential drug delivery device. J Phys Chem C 2007; 111:8437-42
13. Shen W, Xiong H, Xu Y, et al. ZnOpoly(methyl methacrylate) nanobeads for enriching and desalting low-abundant proteins followed by directly MALDI-TOF MS analysis. Anal Chem 2008; 80:6758-63
14. Abercrombie M, Ambrose EJ. The surface properties of cancer cells: a review. Cancer Res 1962; 22:525-48 cancerres.aacrjournals.org

15. Bockris JOM, Habib MA. Are there electrochemical aspects of cancer? Journal of Biological Physics 1982; 10:227-37

16. Papo N, Shahar M, Eisenbach L, Shai Y. A novel lytic peptide composed of DL-amino acids selectively kills cancer cells in culture and in mice. Journal of Biological Chemistry. 2003; 278:21018-23.

17. Wu HQ, Wei XW, Shao MW, Gu JS. Synthesis of zinc oxide nanorods using carbon nanotubes as templates. Journal of Crystal Growth 2004; 265:184-9

18. Wang RM, Xing YJ, and Yu DP. Fabrication and microstructure analysis on zinc oxide nanotubes. N J Phys 2003; 5:115-17

19. Nie L, Gao L, Feng P, et al. Three-dimensional functionalized tetrapod-like ZnO nanostructures for plasmid DNA delivery. Small 2006; 2:621-5

20. Hafeli UO, Riffle JS, Harris-Shekhawat L, et al. Cell uptake and in vitro toxicity of magnetic nanoparticles suitable for drug delivery. Mol Pharm 2009; 6:1417-28

21. Ryter SW, Kim HP, Hoetzel A, et al. Mechanisms of cell death in oxidative stress. Antioxid Redox Signal 2007; 9:49-89

22. Lin W, Xu Y, Huang CC, et al. Toxicity of nano- and micro-sized ZnO particles in human lung epithelial cells. J Nanopart Res 2009; 11:25-39

23. Jeng HA, Swanson J. Toxicity of metal oxide nanoparticles in mammalian cells. J Environ Sci Health A Tox Hazard Subst Environ Eng 2006; 41:2699-11

24. Mortimer M, Kasemets K, Kahru A. Toxicity of ZnO and CuO nanoparticles to ciliated protozoa Tetrahymena thermophila. Toxicology 2010; 269:182-9

25. Franklin NM, Rogers NJ, Apte SC, et al. Comparative toxicity of nanoparticulate ZnO, bulk ZnO, and ZnCl2 to a freshwater microalga (Pseudokirchneriella subcapitata): the importance of particle solubility. Environ Sci Technol 2007; 41:8484-90